Dicle University
Journal of Engineering
https://dergipark.org.tr/tr/pub/dumf
duje.dicle.edu.tr

Research Article

Design Optimization and Material Innovation for the 463L Air Cargo Pallet

Burak ŞAHİN[1*], Erkan SÖYLEMEZ[2]

[1] Gaziantep University, Aerospace Engineering Department, buraksahin@gantep.edu.tr, Orcid No: 0000-0002-8666-4902
[2] Gaziantep University, Aerospace Engineering Department, soylemezerkan27@gmail.com, Orcid No: 0009-0002-3575-0613

ARTICLE INFO

Article history:

Received 12 January 2026
Received in revised form 21 April 2026
Accepted 12 May 2026
Available online 12 July 2026

Keywords:

463L air cargo pallet, Composite core design, Finite element analysis, Weight reduction, Aircraft performance

Doi: 10.24012/dumf.1860770

* Corresponding author

ABSTRACT

This study presents a design optimization and material innovation approach for the 463L air cargo pallet, aiming to improve structural efficiency while maintaining operational reliability. The conventional pallet, which incorporates a balsa wood core, suffers from inherent limitations such as density variability, environmental sensitivity and conservative mass allowances that reduce effective payload capacity. To address these issues, a redesigned pallet configuration was developed by integrating a grid-type core geometry combined with a polypropylene reinforced with 30 percent glass fiber composite material. Finite element analyses were conducted under three critical loading scenarios representing ground and in-flight conditions. The numerical model was validated through mesh convergence and comparison with literature on sandwich structures. The results indicate that the redesigned pallet exhibits a stable and predictable structural response, with only a moderate increase of approximately 4 to 5 percent in both maximum deflection and stress compared to the conventional design. Despite these slight increases, the proposed design achieves significant improvements in structural efficiency. The total mass is reduced by 7.94 percent, corresponding to 10.41 kg, while the pallet thickness is decreased by 27.15 percent. Additionally, the use of a homogeneous composite core eliminates variability in material properties, enhances resistance to environmental degradation, and improves consistency in mass distribution. Overall, the proposed design demonstrates a favorable engineering trade-off, where minor increases in deformation and stress are offset by substantial gains in weight reduction, thickness optimization, and operational performance. These improvements directly contribute to increased payload capacity, improved stacking efficiency, and enhanced reliability in air cargo operations.

Introduction

Air cargo transportation systems require highly efficient, reliable and standardized load-handling solutions to meet the increasing demands of modern logistics operations. Among these, palletized cargo systems play a critical role in ensuring rapid deployment, operational flexibility, and compatibility across different aircraft platforms. In particular, the 463L air cargo pallet has become a cornerstone of military and commercial air transport due to its robust design and long-standing operational use. However, evolving performance requirements, including weight reduction, structural efficiency and durability, have necessitated a more detailed examination of its current configuration. In this context, a comprehensive understanding of the structural characteristics, functional components, and inherent limitations of the existing pallet design is essential before proposing any optimization or redesign approach. This section provides a detailed overview of the 463L air cargo pallet, specifically the HCU-6/E model by consisting of the pallet system structure, key design features and the load cases to which the pallet is subjected. Furthermore, the inherent limitations and shortcomings of the current design are highlighted. The 463L pallet is a standardized air cargo pallet used mostly for military and moderately for commercial air cargo transport. A standardized pallet system is essential for the efficiency of air cargo transport infrastructure (Figure 1). The primary aim is that it enables unitized loading and handling across different aircraft types with minimal variation. Another critical factor is its reliability and widespread availability, making it suitable for most operational contexts. The pallet was originally developed in the late 1950s and has been in active use since April 1963. The designation “463L” reflects this origin, where “463” denotes the fourth month of the year 1963 and the letter “L” represents “Logistics” [1]. The pallet consists of a balsa wood core sandwiched between aluminum skins from the top and bottom, a frame of aluminum rail around the edges of the core and tiedown rings attached to the rail. The balsa wood core shows high strength to mass ratio properties, which is crucial for the application in a cargo pallet. The top and bottom aluminum skins are enhancing the strength of the pallet, protecting the balsa wood core from wear and impacts. The rails around the side of the pallet are needed for the fixation of the pallet in the cargo hull of an aircraft. The rails on the pallet will interfere with rails mounted on the aircraft floor to restrict the movement of the pallet by its sides. After the pallet is placed along the rails on the aircraft, movement to its sides and upwards will be restricted. Only the movement along the rails will be free, which is needed while the loading and unloading of the cargo hull. This movement will be restricted later on, with different methods like hooks or locking pins after the loading process is completed. The tiedown rings are placed along the rail and around the pallet. These tiedown rings are used for securing cargo nets, which enclose the load and give multiple anchor points for straps which are used for further fixation of the pallet like explained [2]. Figures 1 through 6 illustrate the primary components of the pallet system. The numbered annotations correspond to the elements are given in Table 1. For clarity and relevance, certain details in the drawings have been simplified or omitted. The unmodified versions of these drawings can be found in the cited references [1, 2].

Table 1. The pallet components

1	Top aluminum skin	8	Blind bolt in the tie-down ring assembly
2	Bottom aluminum skin	9	Clip (angle bracket reinforcing the pallet corners)
3	Balsa wood core	10	Blind bolt for the clip
4	Aluminum rail (long side)	11	Restraining rail on the aircraft
5	Aluminum rail (short side)	12	Cargo top net
6	Blind rivet (mounting the skins to the rails),	13	Cargo fixing strap
7	Tie-down ring assembly	14	Pallet roller positions (facilitating smooth and efficient loading/unloading of pallets).

The outer dimension of the pallet is 2743.20 millimeter (mm) in length, 2235.20 mm in width and 57.15 mm in thickness (Figure 7). The usable dimension on the top surface is 2641.6 mm in length and 2133.3 mm in width. The top skin has a thickness of 1.60 mm, the bottom skin a thickness of 2.03 mm and the balsa wood core a thickness of 53.52 mm [2,3]. According to references [3] and [5], the estimated masses of the individual components are summarized in Table 2. Based on these values, a residual mass allowance of 5.48 kg remains for the adhesive applied between interfacing surfaces, the sealant used to fill corner gaps in the rails and the variability arising from the irregular mass distribution of the balsa core.

Owing to this inherent variability, each pallet exhibits a slightly different final mass. Since this irregularity cannot be predicted, the 5.48 kg allowance is conservatively assigned to the adhesive applied across all core surfaces, as also approximated in reference [3]. This margin is constrained by the maximum tare mass limit of the 463L pallet, which is specified as 136.07 kg. Pallets exceeding this threshold after manufacturing are excluded from operational use. In practice, pallets with a tare mass between 130.59 kg and 136.07 kg are considered acceptable;however, for standardization and safety purposes, 136.07 kg is adopted as the nominal tare mass for all pallets [2,3].

In addition to studies focusing on conventional pallet systems [1-16], extensive research has been conducted on the structural behavior of sandwich structures, which share similar load-carrying mechanisms with air cargo pallets. H. M. Öztemiz and Ş. Temiz investigated the bending behavior of sandwich panel composites using both experimental and finite element approaches, demonstrating that accurately defined material models, boundary conditions, and mesh refinement can reliably predict deformation responses [17]. Similarly, M. F. Gomaa et al. conducted finite element analyses on sandwich panels subjected to out-of-plane bending and reported a strong agreement between numerical and experimental results [18]. Furthermore, K. Ç. Çıbıkçı highlighted the effectiveness of finite element methods in capturing the dynamic and structural response of sandwich systems, emphasizing the importance of model validation and mesh convergence [19]. Recent studies have highlighted the critical importance of accurately predicting displacement and stress fields in sandwich structures due to their complex failure mechanisms and heterogeneous nature. Advanced finite element approaches, particularly the inverse Finite Element Method, have been shown to provide reliable full-field structural response reconstruction from limited strain data. However, classical formulations may be insufficient for thick or highly heterogeneous laminates. To overcome this limitation, refined formulations incorporating advanced kinematic theories have been developed, significantly improving prediction accuracy for sandwich-type structures [20]. Finite element-based studies have demonstrated that key parameters such as face sheet thickness significantly influence deformation, stress distribution and dynamic behavior. In particular, increasing face sheet thickness leads to reduced deformation and improved structural stiffness, while stress concentrations are typically localized near boundary regions. These findings confirm that validated numerical approaches provide a reliable framework for analyzing and optimizing sandwich-type structures under complex loading conditions [21]. These studies collectively confirm that finite element-based approaches provide a robust and reliable framework for evaluating sandwich-type structures, thereby supporting their application in the structural assessment and optimization of air cargo pallet systems.

The primary motivation of this study is to enhance capacity and operational safety in air cargo transportation for both military and civil applications. Achieving this objective requires a systematic evaluation of existing cargo transport systems to identify critical components with the potential for performance improvement. Within this framework, the 463L air cargo pallet emerged as a key structural element due to its central role in load handling and distribution. Consequently, this study focuses on developing and evaluating a redesigned pallet configuration aimed at improving structural efficiency and overall operational performance. The aim of the study is, attempting to overcome stated weaknesses by design optimization and material innovation. To validate the made changes in the design and material selection, part modelling and finite element analysis tools were used.

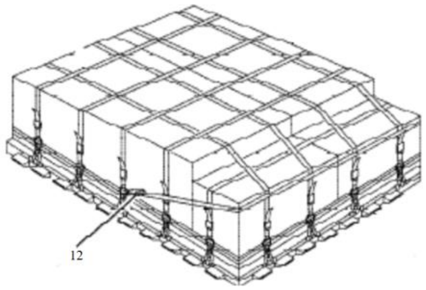

Figure 1. Typical palletized cargo with top net attached [2]

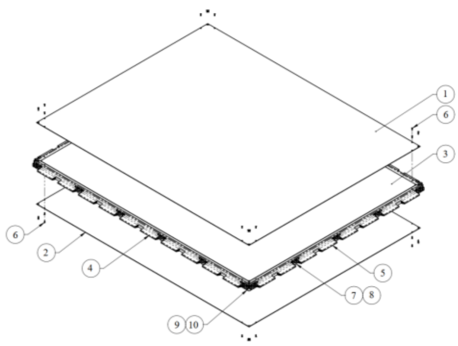

Figure 2. 463L pallet exploded view [3]

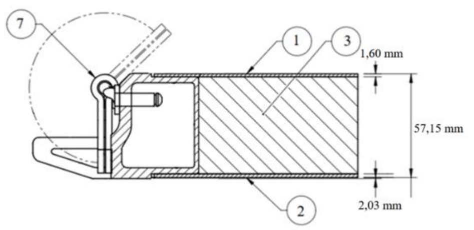

Figure 3. Cross-sectional view of the 463L pallet [3]

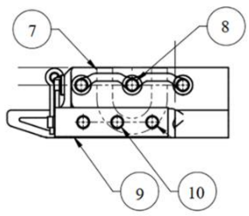

Figure 4. Corner section of the 463L pallet [3]

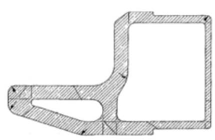

Figure 5. Cross-sectional view of the 463L pallet rail [4]

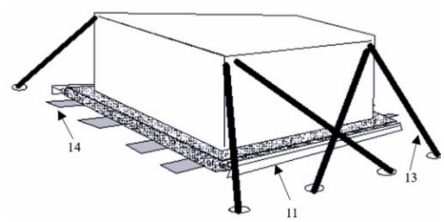

Figure 6. Palletized cargo restrained to the aircraft floor rings with straps [2]

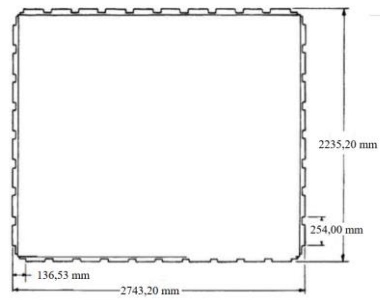

Figure 7. Plan view and dimensions of the 463L pallet [2]

Material and Method

The mechanical and physical properties for the balsa wood core were taken from the references [6] and [7]. The properties were taken according to the density of the balsa wood core, calculated from its mass and volume like shown in Equation 1. The maximum mass capacity of the pallet on its usable top surface is 4535.92 kg. The tiedown rings have a maximum mass capacity at tension, in all directions of 3401.94 kg [2]. Material properties of used materials are given in Table 3 for the finite element analysis. The mechanical and physical properties of the Aluminum 6061-T6 were taken from the ANSYS material properties data without changing, after accuracy was checked. For the safe structural design of an air cargo pallet, including the 463L model, the following load cases must be satisfied [2]:

Case 1: Maximum load on the ground under a gravitational acceleration of 1 g,

Case 2: Maximum load in flight under a downward gravitational acceleration of 4.5 g,

Case 3: Maximum load in flight under a downward gravitational acceleration of 4.5 g, with the application of a safety factor of 1.5, corresponding to 6.75 g.

The limitations which were taken into consideration for design of the current 463L pallet were listed below:

1) Reduced payload capacity due to additional tare mass:

The additional tare mass allowance applied even to lighter pallets reduces the effective payload capacity of the aircraft.

2) Limitations of the balsa wood core:

The mechanical performance of the balsa wood core is highly sensitive to environmental and biological factors including humidity, exposure to chemicals and internal defects formed during tree growth. Being a natural material, it is also susceptible to insect damage, particularly when surface skin delamination occurs. Furthermore, under scenarios where the pallet is dropped into water or exposed to humid conditions, the high moisture absorption capacity of balsa leads to an increase in mass and a deterioration of its mechanical properties.

Table 2. The masses of the pallet components

Component	Mass (kg)	Component	Mass (kg)
Top Skin (Aluminium 6061-T6)	23.76	Rivet (Blind)	32 x 0.0009
Bottom Skin (Aluminium 6061-T6)	30.18	Tiedown Ring Assembly	22 x 0.11
Core (Balsa Wood)	44.29	Bolt in the Tiedown Ring Assembly (Blind)	4 x 0.099
Rail (Aluminium 6061-T6, Long Side)	2 x 8.12	Clip (Angle)	
Rail (Aluminium 6061-T6, Short Side)	2 x 6.53	Bolt for the Clip (Blind)	24 x 0.099
		Total mass of 130.59 kg	

$$density = \frac{mass}{volume} = \frac{44.29}{2.6416*2.1336*0.05352} \quad (1)$$

$$density = 146.83 \ \mathrm{kg/m^3}$$

3) Non-uniformity and anisotropy of balsa wood:

Balsa wood is inherently anisotropic, resulting in variable load-carrying capacities among pallets. Moreover, density variations across natural cores make it nearly impossible to achieve a uniform mass. While the nominal standard mass of the 463L pallet is specified as 131.54 kg, this value cannot be consistently achieved. Consequently, a maximum tare mass limit of 136.07 kg has been established, allowing pallets within this 4.53 kg tolerance band to be approved for use [2]. This variability creates two major issues:

- Reduced effective payload:

To account for the worst-case scenario, cargo-loading guidelines adopt 136.07 kg as the reference tare mass for every pallet [8]. When pallets are actually lighter, this conservative assumption directly decreases the aircraft's overall payload capacity, as each pallet is penalized by up to 4.53 kg of unused allowance.

- Errors in center-of-gravity calculations:

Accurate determination of the aircraft's center of gravity is critical for both flight safety and performance. By uniformly assigning the maximum tare mass, even when unnecessary, cargo loading may become unbalanced. Such imbalance may cause reduced aircraft performance in the best case, and in the worst case could contribute to catastrophic accidents.

Table 3. The mechanical properties of Balsa, Aluminum 6061-T6 and PP-GF30

	Balsa	Al 6061-T6	PP-GF30
Density (kg/m^3)	146.83	2713	1140
Young's modulus (GPa)	0.1863 [6]	69.04	6.33
Poisson's ratio	0.229 [7]	0.33	0.35
Ultimate compressive strength (MPa)	1.1 [6]	313.10	71.7

4) Constraints due to pallet thickness:

The current pallet thickness restricts stacking efficiency. A reduction in thickness would enable greater stacking height and, consequently, improved cargo volume utilization. For modelling, firstly, a physical test environment was selected. In this case is the cargo hull of the C5 – Galaxy cargo aircraft was selected, due to its large 463L pallet capacity of 36 pallets [9]. Secondly the current pallet was modelled in a CAD software. Then load surfaces and fixture surfaces for the analysis were defined.

After these steps, maximum deformation values under maximal mass and gravitational acceleration capacity were extracted. These values set a maximum deflection value for the newly purposed design and made iterating among values easier. To define the test environment of the C5 – Galaxy aircraft and to implement it to the analysis, its layout and dimension of its rollers [2] is needed. These dimensions correspond to the fixed support surfaces on the bottom of the pallet which are shown in following figure (Figure 8).

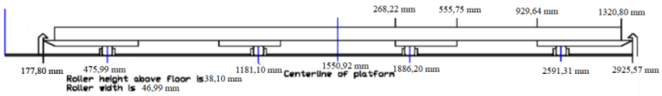

Figure 8. Roller Layout of the C5 – Galaxy aircraft

Finite Element Modeling and Validation

The numerical analyses were carried out using the finite element method implemented in ANSYS Workbench 2019. The geometric model of the pallet was created using SolidWorks and imported into ANSYS for structural analysis.

The finite element model was discretized using SOLID186 elements, which are higher-order 3D 20-node structural elements suitable for capturing complex stress and deformation distributions.

In addition, contact interactions between different structural components were modeled using CONTA174 (contact elements) and TARGE170 (target elements). Surface-to-surface contact formulations were defined to ensure proper load transfer between bonded regions. The interactions between different structural components were defined using a bonded contact formulation, assuming perfect adhesion between the layers. In this approach, no relative motion or separation is allowed between contacting surfaces, ensuring full transfer of stresses and strains across the interfaces.

Loading and Boundary Conditions

The loading and boundary conditions were defined to accurately represent the operational constraints of the 463L air cargo pallet within the aircraft cargo system. Three different load cases as discussed above are prepared for the analysis. In this section the corresponding pressure values over the usable surface area of the pallet for these load cases were calculated by depending on force and area. These pressure values of 7.895 kPa, 35.528 kPa and 53.292 kPa were applied in a constant manner respectively for Case 1 (1.0*g), Case 2 (4.5*g) and Case 3 (6.75*g) respectively across the surface area denoted with the letter "I" from Figure 9-10.

As stated earlier, the first fixed surfaces to be considered during the analysis, are the surfaces where the rollers of the aircraft support the pallet from the bottom (E, F, G and H are showing the dedicated surfaces. Secondary section to consider, is the frame of rails around the lateral surface of the pallet. These surfaces were fixed, due to its mechanical restriction by the rails. (A, B, C, and D are showing the dedicated surfaces in Figure 9 and Figure 10).

A uniformly distributed pressure load was applied on the top usable surface of the pallet, representing the cargo load. The magnitude of the applied pressure was calculated based on the maximum payload capacity and corresponding gravitational accelerations. Three loading cases were considered: Case 1: 1 g (7.895 kPa), Case 2: 4.5 g (35.528 kPa) and Case 3: 6.75 g (53.292 kPa). The pressure loads were applied consistently over the designated loading surface. The boundary conditions were defined based on the mechanical constraints of the pallet within the aircraft cargo system. Fixed support conditions were applied at two main regions: The bottom support regions, corresponding to the contact surfaces between the pallet and the aircraft roller system: The lateral rail surfaces, representing the restriction imposed by the aircraft side rail mechanism and these constraints prevent translational and rotational motion in all directions at the defined regions.

To ensure the correctness of the applied loading and boundary conditions, the reaction forces at the supports were checked and found to be consistent with the applied loads, confirming equilibrium of the system. Both the loading surfaces and fixed support regions are illustrated in Figure 9-10.

Mesh convergence

A mesh convergence study was performed to evaluate the influence of element size on the maximum deformation results. The analysis was conducted using different mesh sizes ranging from 8 mm to 100 mm as given in Figure 11. The results indicate that the deformation values obtained for element sizes of 8, 9, and 10 are very close to each other, with successive changes remaining below 1%. This demonstrates that mesh-independent results are achieved within this range. Element size, nodes and elements were obtained as 10 mm, 3137368 nodes and 610884 elements respectively. Boundary conditions were verified by ensuring that the reaction forces are consistent with the applied loads (Figure 12).

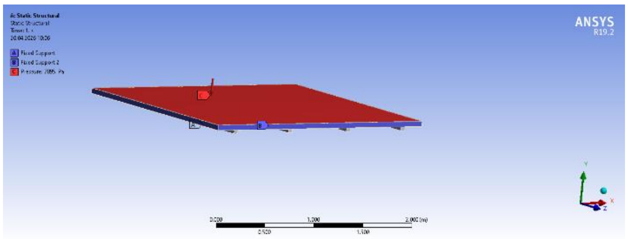

Figure 9. Fixed support and pressure surfaces (View 1)

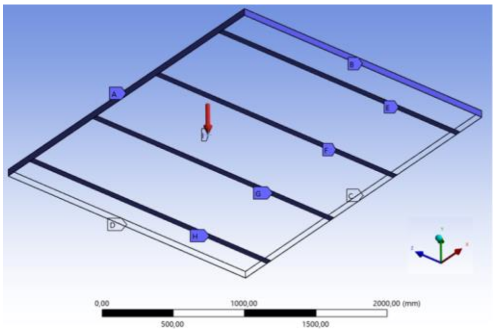

Figure 10. Fixed support and pressure surfaces (View 2)

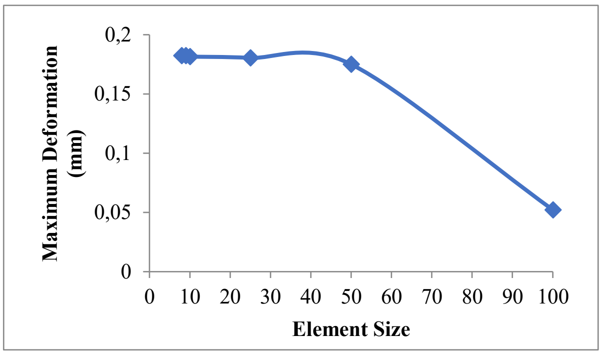

Figure 11. Mesh convergence analysis

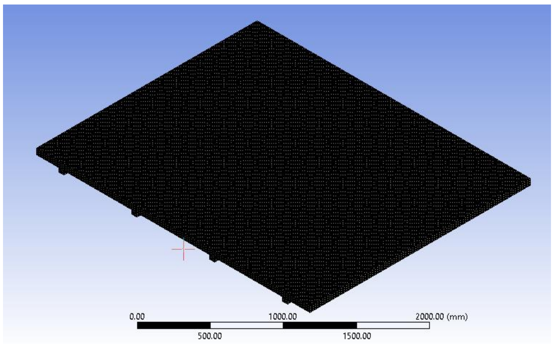

Figure 12. Finite element mesh of the pallet model

Model Validation

To verify the accuracy of the developed finite element model, validation research was conducted using previously published results on sandwich structures. Öztemiz and Temiz analyzed the bending behavior of composite sandwich panels using both experimental and finite element approaches. The authors demonstrated that finite element models can accurately predict deformation behavior when appropriate material modeling, mesh density, and boundary conditions are applied [17]. Similarly, a finite element model of sandwich panels developed in ANSYS was validated against experimental data, showing a good agreement between numerical and experimental deflection results [18].

In the present study, the numerical modeling approach follows similar assumptions, including: linear elastic material behavior, bonded interfaces between layers and appropriate mesh refinement (validated via mesh convergence study). The deformation values obtained in this study fall within the range reported in the literature for comparable sandwich structures under similar loading conditions. Moreover, previous studies in the literature have reported that well-established finite element models of sandwich structures typically exhibit deviations within 3–10% when compared with experimental or reference results, confirming the reliability of such numerical approaches [19]. Based on these comparisons, the developed numerical model is considered to be sufficiently accurate and reliable for evaluating the structural performance of the proposed design.

Results and Discussion

The structural response of the current pallet design under different loading conditions is summarized in Table 4 and 5, while the corresponding deflection and equivalent (von Mises) stress distributions are presented in Figure 13–18. As expected, both the maximum deflection and stress increased with increasing applied load, exhibiting a consistent and predictable trend. Under a gravitational acceleration of 1 g, corresponding to an applied pressure of 7.895 kPa, the pallet exhibited a maximum deflection of 0.18156 mm (≈181.56 μm). This relatively small displacement indicates a high stiffness of the structure under static ground loading conditions and confirms that the pallet easily satisfies baseline operational requirements. When the loading increased to 4.5 g (35.528 kPa), the maximum deflection reached 0.81701 mm (≈817.01 μm). Although this represents a significant increase compared to the 1 g case, the deformation remains within acceptable serviceability limits, demonstrating the capability of the pallet to withstand dynamic in-flight loading conditions, such as turbulence-induced accelerations. In the most critical loading scenario, where a safety factor of 1.5 was applied to the 4.5 g condition (resulting in 6.75 g and 53.292 kPa), the maximum deflection increased to 1.2255 mm (≈1225.5 μm). Despite this substantial increase, no structural instability or failure was observed. The deformation contours reveal that the maximum displacement consistently occurred in the central regions of the pallet (Figure 13–15), where bending effects are dominant. Importantly, the deformation mode remained unchanged across all loading cases, with only the magnitude of displacement increasing. This indicates that the structural behavior of the pallet is stable and governed by a consistent load-transfer mechanism.

A similar trend was observed in the stress analysis. The maximum von Mises stress values increased from 13.381 MPa at 1 g to 60.217 MPa at 4.5 g and reached 90.326 MPa at 6.75 g. This progressive increase closely follows the applied load and deflection trends, indicating an approximately linear elastic response of the structure. The stress distributions (Figure 16–18) show that critical stress concentrations are primarily localized in regions responsible for load transfer to the supports. With increasing load levels, the stress intensity in these regions becomes more pronounced; however, the overall distribution pattern remains consistent, and no unexpected stress concentrations develop.

Overall, the results demonstrate that the current 463L pallet design exhibits a predictable, stable, and predominantly elastic structural response under all considered loading scenarios. The nearly linear relationship between applied load, deformation, and stress confirms that the structure operates within the elastic regime. While the increase in deflection under higher accelerations highlights the importance of serviceability considerations, the absence of critical stress concentrations or instability mechanisms confirms that the design satisfies both strength and stiffness requirements. These findings validate the current configuration for safe operational use and provide a robust foundation for future optimization studies aimed at reducing structural weight while maintaining or enhancing mechanical performance.

In addition to the previous analyses of the conventional pallet configuration, a redesigned pallet core (Figure 19) was developed with the primary objectives of weight reduction and improved structural efficiency. This was achieved by introducing a grid-like core structure formed by systematically removing rectangular and horizontal sections from the original solid core in controlled increments.

Table 4. Maximum deflection results of the current pallet design in different load cases

Case	Applied load (g)	Applied Load (kPa)	Maximum Deflection (mm)
1	1	7.895	0.18156
2	4.5	35.528	0.81701
3	6.75	53.292	1.22550

Table 5. Maximum stress (Von-Misses) results of the current pallet design in different load cases

Case	Applied load (g)	Applied Load (kPa)	Maximum Stress (MPa)
1	1	7.895	13.381
2	4.5	35.528	60.217
3	6.75	53.292	90.326

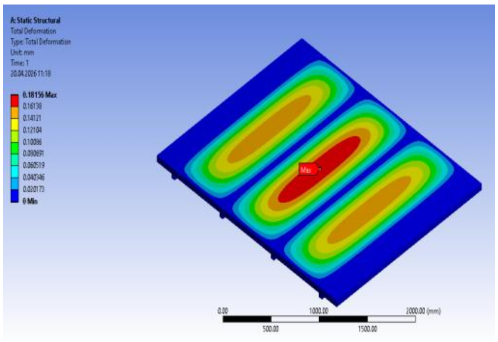

Figure 13. Deformation distribution of the current pallet under 1 g loading

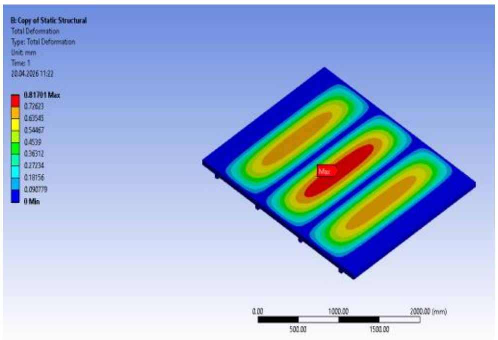

Figure 14. Deformation distribution of the current pallet under 4.5 g loading

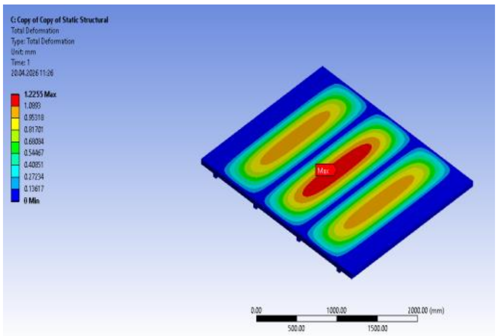

Figure 15. Deformation distribution of the current pallet under 6.75 g loading

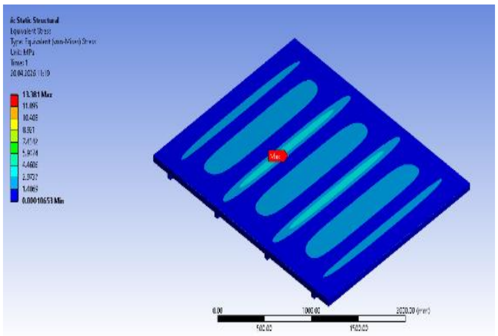

Figure 16. Equivalent (von Mises) stress distribution of the current pallet under 1 g loading

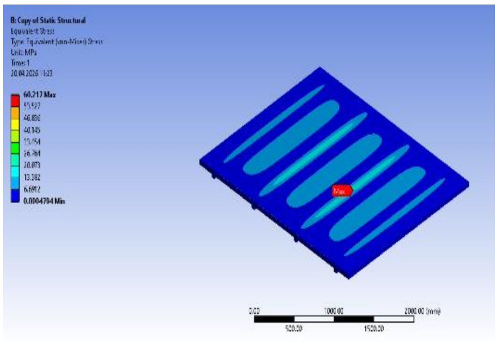

Figure 17. Equivalent (von Mises) stress distribution of the current pallet under 4.5 g loading

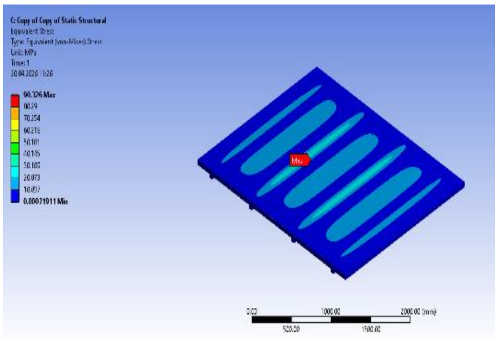

Figure 18. Equivalent (von Mises) stress distribution of the current pallet under 6.75 g loading

The geometric parameters of this new core configuration (Figure 19) were iteratively optimized until the resulting deformation levels approached those of the baseline design while maintaining structural stability. To complement the geometrical modification, a material with a favorable strength-to-weight and stiffness-to-density ratio were required. Based on a comparative evaluation of candidate polymers and reinforced polymers, polypropylene reinforced with 30% glass fiber (PP–GF30) was selected.

The material properties used in the finite element analyses adopted from the literature [10–16] were given in Table 3. The redesigned pallet (Figure 20) was analyzed under the same loading and boundary conditions as the conventional configuration to enable a direct comparison. The structural response of the new design is summarized in Tables 6 and 7, with deformation (Figure 21-23) and stress distributions presented in Figure 24–26. Similar to the baseline design (current pallet), both maximum deflection and von Mises stress increased with increasing applied load, indicating a consistent and predictable mechanical behavior. Under static ground loading (1 g, 7.895 kPa), the maximum deflection of the redesigned pallet was calculated as 0.19073 mm (≈190.73 µm). Although this value is slightly higher than that of the conventional design, it remains within a very limited range, confirming sufficient stiffness under baseline operating conditions. For the in-flight loading scenario (4.5 g, 35.528 kPa), the maximum deflection reached 0.85831 mm (≈858.31 µm), while under the most critical loading case (6.75 g, 53.292 kPa), the deflection increased to 1.2875 mm (≈1287.5 µm) (Table 6). Despite this increase, no structural instability or failure modes were observed. The deformation contours consistently indicate that the maximum displacement occurs in the central regions of the pallet, governed by bending-dominated behavior, and the deformation mode remains unchanged across all loading cases. The stress analysis further supports these findings (Table 7). The maximum von Mises stress values increased from 14.033 MPa at 1 g to 63.149 MPa at 4.5 g and reached 94.724 MPa at 6.75 g.

These values are moderately higher than those of the conventional pallet, which can be attributed to the reduced material volume and altered load paths introduced by the grid-like structure. Nevertheless, the stress increase follows an approximately linear trend with applied load, indicating that the redesigned structure operates predominantly within the elastic regime. The stress distributions reveal that critical stress concentrations remain localized in primary load transfer regions, and no unexpected stress intensification or failure-prone zones emerge.

Table 6. Maximum deflection results of the new pallet design in different load cases

Case	Applied load (g)	Applied Load (kPa)	Maximum Deflection (mm)
1	1	7.895	0.19073
2	4.5	35.528	0.85831
3	6.75	53.292	1.2875

Table 7. Maximum Stress (Von-Misses) of the new pallet design in different load cases

Case	Applied load (g)	Applied Load (kPa)	Maximum Stress (MPa)
1	1	7.895	14.033
2	4.5	35.528	63.149
3	6.75	53.292	94.724

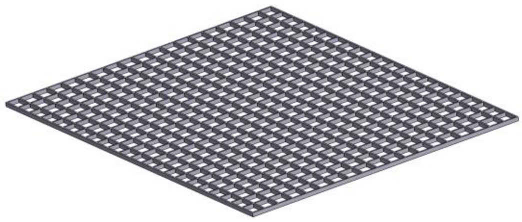

Figure 19. The new core for the pallet

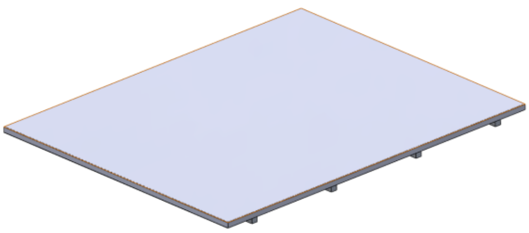

Figure 20. Cross-sectional views of the pallet with new core

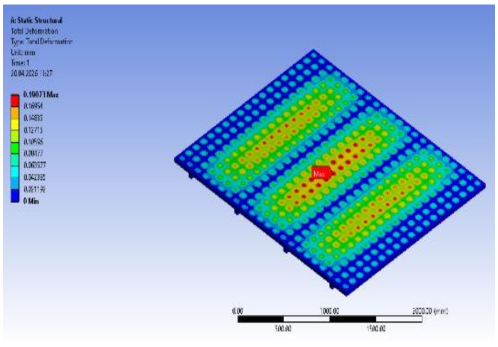

Figure 21. Deformation distribution of the new pallet under 1 g loading

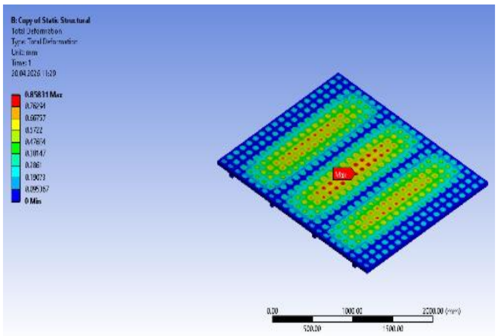

Figure 22. Deformation distribution of the new pallet under 4.5 g loading

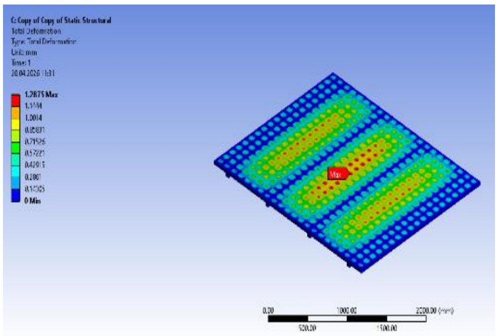

Figure 23. Deformation distribution of the new pallet under 6.75 g loading

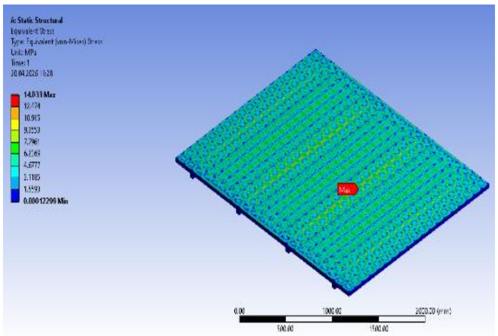

Figure 24. Equivalent (von Mises) stress distribution of the new pallet under 1 g loading

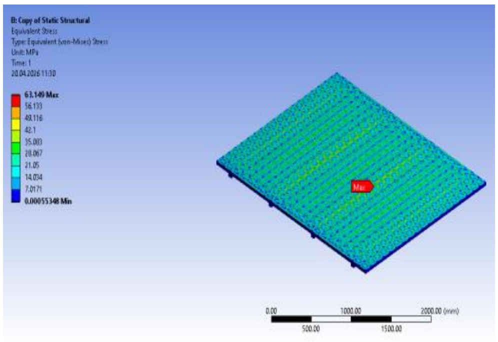

Figure 25. Equivalent (von Mises) stress distribution of the new pallet under 4.5 g loading

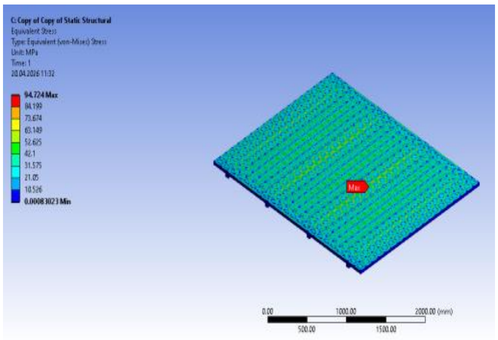

Figure 26. Equivalent (von Mises) stress distribution of the new pallet under 6.75 g loading

Overall, the redesigned pallet exhibits a stable and predictable structural response under all considered loading conditions. While the new configuration results in slightly higher deflection and stress values compared to the conventional design, it successfully meets both strength and serviceability requirements. Importantly, these results indicate that the geometric and material modifications achieve a more efficient structural design, likely associated with weight reduction, without compromising mechanical integrity. Consequently, the proposed pallet configuration provides an effective alternative to the conventional 463L design, offering improved structural efficiency and potential operational advantages such as enhanced payload capacity and reduced material usage. Further optimization efforts may focus on refining local stress concentrations and enhancing stiffness to fully exploit the benefits of the redesigned architecture.

A systematic comparison of the previously identified weaknesses and the corresponding improvements achieved by the new design is presented below.

Excess tare mass due to variability in balsa wood density

This limitation is effectively eliminated in the redesigned pallet. The PP–GF30 composite core exhibits a fixed and uniform density, ensuring consistency across all pallets. Consequently, the conservative mass allowance previously required to compensate for the natural variability of balsa wood is no longer necessary. According to the results (Figure 27 and Table 10), the redesigned pallet achieves a total mass reduction of 10.41 kg, corresponding to 7.94%. This reduction becomes significantly more impactful when scaled to full aircraft loading configurations, directly contributing to increased payload capacity and improved operational efficiency.

Degradation of strength due to humidity, chemicals, and natural defects:

The dependency on natural wood has been completely removed. Unlike balsa, which is highly sensitive to moisture absorption, internal defects and biological degradation, the PP–GF30 composite core provides enhanced resistance to environmental and chemical effects. This results in improved durability and long-term structural reliability under varying operational conditions.

Non-uniform strength properties among pallets

The inherent variability of balsa wood previously resulted in inconsistent mechanical properties and mass distribution between pallets. The redesigned pallet eliminates this issue by utilizing a homogeneous composite material with uniform density and predictable mechanical behavior. This uniformity significantly reduces uncertainties in structural performance and improves the accuracy of aircraft center-of-gravity calculations. Consequently, potential imbalances arising from uneven pallet masses are mitigated, enhancing both flight safety and operational precision.

Limitations due to pallet thickness

The redesigned pallet addresses this limitation by achieving a thickness reduction of 27.15% (15.52 mm), decreasing from 57.15 mm to 41.63 mm (Figure 21 and Table 10). This substantial geometric improvement enables increased stacking efficiency and more effective utilization of cargo volume, which is particularly critical in aircraft with strict dimensional constraints.

The mass reduction is primarily attributed to the optimization of key structural components, as given in Table 10. The core mass decreased by 4.83%, while the aluminum rails exhibited reductions of approximately 13% for both long and short sections due to the reduced pallet thickness. The most significant contribution arises from the adhesive, where an 80.47% reduction was achieved. This reduction is directly related to the decreased surface area of the grid-type core structure, which requires substantially less bonding material compared to the solid balsa configuration. From a structural performance perspective, it is important to interpret these improvements together with the mechanical response of the redesigned pallet. As previously discussed, the new configuration exhibits a moderate increase of approximately 4–5% in both maximum deflection and von Mises stress across all loading conditions. This behavior is a direct consequence of reduced material volume and localized stiffness variations introduced by the grid-type architecture.

However, these increases remain limited and within acceptable serviceability and strength limits. The stress levels are well below the material capacity, and the structure continues to operate entirely within the elastic regime. Moreover, the deformation patterns and stress distributions remain consistent with those of the conventional design, indicating that the fundamental load transfer mechanism is preserved.

Overall, the redesigned pallet demonstrates a favorable engineering trade-off, where a minor and controlled increase in deformation and stress is accompanied by substantial gains in weight reduction, thickness optimization and material uniformity. These improvements not only enhance structural efficiency but also provide significant operational advantages, including increased payload capacity, improved stacking capability and enhanced durability.

Table 8. Comparison of maximum deformations

Case	Deflection of Current Pallet Design (mm)	Deflection of New Pallet Design (mm)	Difference %
1 g	0,18156	0,19073	4,808
4.5 g	0,81701	0,85831	4,812
6.75 g	1,2255	1,2875	4,816

Table 9. Comparison of maximum stress (Von-Misses)

Case	Maximum Stress (Von-Misses) of Current Pallet Design (MPa)	Maximum Stress (Von-Misses) of New Pallet Design (MPa)	Difference %
1 g	13,381	14,033	4,646
4.5 g	60,217	63,149	4,643
6.75 g	90,326	94,724	4,643

According to the assembly manual, the adhesive is applied to every six surfaces of the balsa wood core [3]. The outer surface areas of both current design and new design, were easily retrieved from the modelling program SolidWorks. The difference in the surface areas (outer surface areas for the grid) were put in a rate to the mass of the adhesive, so the new mass of the adhesive was calculated.

In terms of mass distribution, the redesigned pallet achieved a total mass reduction of 7.94 %, corresponding to 10.41 kg less than the current design (Table 10). The most notable savings were realized in the shortened aluminum rails (≈13% reduction) and adhesive requirements (≈80% reduction). These reductions also contributed to a more uniform mass distribution among pallets, an important factor for ensuring accurate center of gravity calculations during cargo loading. Furthermore, the redesigned pallet thickness decreased by 27.15% (from 57.15 mm to 41.63 mm) enabling more efficient stacking height and cargo volume utilization (Figure 28 and Table 10).

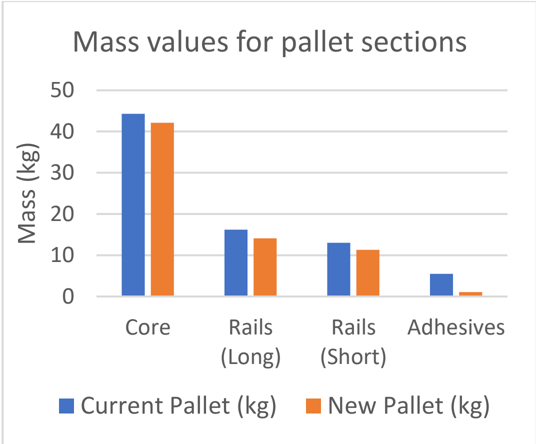

Figure 27. Mass values comparison chart

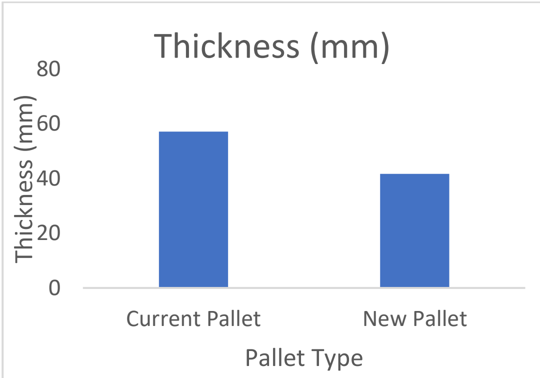

Figure 28. Thickness change comparison chart

Table 10. Comparison of maximum deformations

Part	Current Pallet (kg)	New Pallet (kg)	Diff. (kg)	Diff. in %
Top Skin	24,46	24,46	+/- 0 *	0 % *
Bottom Skin	24,46	24,46	+/- 0 *	0 % *
Core	44,29	42,15	- 2,14	4,83 % less
Rails (Long)	16,24	14,13	- 2,11	12,93% less
Rails (Short)	13,06	11,31	- 1,75	13,39% less
Rivets	0,0288	0,0288	+/- 0 *	0 % *
Tiedown Rings	2,42	2,42	+/- 0 *	0 % *
Clips (Angle)	0,396	0,396	+/- 0 *	0 % *
Clip Bolts	0,216	0,216	+/- 0 *	0 % *
Adhesives	5,48	1,07	- 4,41	80,47 % less
TOTAL	131,05	120,64	- 10,41	7,94 % less
Thickness	57,15 mm	41,63 mm	-15,52 mm	27,15 % less

* = No changes on these parts were done, they have been kept constant.

Conclusion

This study demonstrated that the structural performance of the 463L air cargo pallet can be significantly enhanced through a combined approach of geometric optimization and material substitution. The replacement of the conventional balsa wood core with a PP–GF30 composite and the introduction of a grid-type core pattern resulted in a structurally efficient and operationally advantageous design. The numerical analyses confirmed that the redesigned pallet maintains a stable and predictable elastic response under all considered loading conditions. Although the new configuration exhibits a moderate increase of approximately 4–5 percent in maximum deflection and von Mises stress, these increases remain within acceptable serviceability and strength limits, and no structural instability or critical stress concentrations were observed. In contrast, substantial improvements were achieved in key performance metrics. The total pallet mass was reduced by 7.94 percent, eliminating the need for conservative mass allowances associated with balsa variability. The thickness reduction of 27.15 percent enables more efficient stacking and improved cargo volume utilization. Furthermore, the use of a homogeneous composite material ensures uniform mechanical properties, reducing uncertainties in structural behavior and significantly improving the accuracy of aircraft center-of-gravity calculations.

From an engineering standpoint, the redesigned pallet represents a well-balanced trade-off, where a minor and controlled increase in deformation and stress is outweighed by considerable gains in weight reduction, geometric optimization, durability, and operational efficiency. These improvements directly translate into enhanced payload capacity, improved logistics performance and increased reliability in air cargo operations. Nevertheless, the present study is inherently limited by its reliance on linear elastic finite element simulations without experimental validation. Critical aspects such as material nonlinearity, progressive damage evolution, interfacial debonding, and impact-induced failure mechanisms were not explicitly considered. In addition, the long-term performance of the PP–GF30 composite under cyclic loading, environmental exposure, and aging conditions remains unquantified. The assumption of perfectly bonded interfaces may also lead to optimistic estimations of load transfer and structural integrity. To address these limitations, future work should prioritize full-scale experimental validation under representative operational conditions, including static, dynamic and impact loading scenarios. Advanced numerical approaches incorporating nonlinear material behavior, damage mechanics, and cohesive interface modeling are required to capture realistic failure modes. Furthermore, fatigue performance, environmental durability and repairability should be systematically investigated to ensure long-term reliability. Additional multi-objective optimization studies focusing on the refinement of the grid-type core geometry may further reduce stress concentrations while preserving weight advantages. Finally, integrating manufacturability, cost-efficiency and certification constraints into the design framework will be essential for transitioning the proposed concept into a practical and deployable aerospace solution.

Ethics committee approval and conflict of interest statement

"There is no need to obtain permission from the ethics committee for the article prepared"

"There is no conflict of interest with any person / institution in the article prepared"

References

1. 463L pallet and dunnage system evaluation, AL/HR-TP-1997-0043, United States Air Force Armstrong Laboratory, USA, 1997

2. Interface standard: designing for internal aerial delivery in fixed wing aircraft, MIL-STD-1971D, United States Department of Defense, USA, 2021

3. Pallet assembly cargo HCU-6E, DWG NO: 7031843, United States Air Force, Warner Robins Air Logistics Centre, USA, 2012

4. Extrusion pallet rail airborne cargo, DWG NO: 7133042, United States Air Force, USA, 2005

5. Engineering study report universal platform and cargo restraint device, AD648986, Books & Perkins Incorporated, Defense Product Division, USA, 1965

6. M. Borrega, L. J. Gibson (2015). Mechanics of balsa (Ochroma pyramidale) wood. Department of Materials Science and Engineering, Massachusetts Institute of Technology.

7. Wood handbook: Wood as an engineering material, United States Department of Agriculture Forest Services, USA, 2021

8. Loading and tiedown procedures for conventional ammunition items on the 463L/Intex pallet for the Comanche and kiowa helicopters," DA 12/1-92, Department of Army Drawing, USA, 1992

9. Air deployment planning guide," GTA 55-07-003, Headquarters: Department of Army, USA, 1996

10. Polypropylene with 30% Glass Fiber Filler," MatWeb material property data, Mar. 1, 2025.

11. Polypropylene with 30 % glass fibre (PP GF30),Kern GmbH, Mar. 5, 2025. [Online].

12. Polypropylene Technical Datasheet. PP-30GF, Smiths metal centres, Mar. 1, 2025.

13. Technical Datasheet for Ultrafuse PP GF30, BASF 3D printing solutions BV, Mar. 3, 2025.

14. PP-30GF Material Datasheet, addimen additive manufacturing, Mar. 3, 2025.

15. Technical Datasheet GEHR PP-30GF," GEHR GmbH, Mar. 3, 2025.

16. Material properties Ultra Wear PP-GF30, POLYTRON Kunststofftechnik GmbH & Co. KG, Mar. 6, 2025.

17. H. M. Öztemiz and Ş. Temiz, "Experimental and FEM investigation of bending behaviors of S-core sandwich panel composites", *International Journal of Solids and Structures*, 286, 2024.

18. M. F. Gomaa, W. A. Attia, and A. H. Amer, "Finite Element Analysis of Out-Of-Plane Bending of Precast Concrete Sandwich Panels", *International Journal Civil Engineering*, vol. 11, no.2, 2020.

19. K. Ç. Çıbıkçı, "Modal Analysis of Sandwich Structure Using Finite Element Approach", *Dicle Üniversitesi Mühendislik Fakültesi Mühendislik Dergisi*, vol. 16, no.3, pp. 717-724, 2025.

20. P. Cerracchio, M. Gherlone, M. Di Sciuva, and A. Tessler, "A novel approach for displacement and stress monitoring of sandwich structures based on the inverse Finite Element Method", *Composite Structures,* vol. 127, pp. 69-76, 2015.

21. S. Upreti, V. K. S,ngh, S. K. Kamal, A. Jain, and A. Dixit, "Modelling and analysis of honeycomb sandwich structure using finite element method", *Materials Today: Proceedings,* vol. 25, pp. 620-625, 2020.